*Journal of Chromatography*, 454 (1988) 23–36
Elsevier Science Publishers B.V., Amsterdam — Printed in The Netherlands

CHROM. 20 776

# STUDY OF THE INJECTION PROCESS IN A GAS CHROMATOGRAPH SPLIT INJECTION PORT

A. E. KAUFMAN* and C. E. POLYMEROPOULOS*
*Department of Mechanical and Aerospace Engineering, Rutgers University, P.O. Box 909, Piscataway, NJ 08855-0909 (U.S.A.)*
(First received January 4th, 1988; revised manuscript received June 22nd, 1988)

## SUMMARY

Pressure and temperature variations which occur during an injection in a gas chromatograph split injection port were measured for different sample sizes, injection port temperatures, solvents, injection port inserts, and split flow-rates. A control volume analysis of the injection process was developed to predict the pressure, temperature and split ratio variations during and after the injection. Comparison of the predicted pressure and temperature results with the experimental measurements was satisfactory. An example is presented demonstrating how the model can be used to predict the quantitative error in a split injection port.

## INTRODUCTION

Split injection is a convenient, widely used sample introduction technique for capillary column gas chromatography. The carrier gas entering the injection port is split into two unequal flows with the smaller flow entering the capillary column, and the ratio of these flows (split flow:column flow) defines the split ratio. Ideally, when the sample is injected, it is split at this preset ratio resulting in a known fraction of the sample passing through the column. Though split injection is based on a very simple concept many problems arise when accurate quantitative results are required. Peak areas may vary by a factor of two from one injection to the next[1] and deviations from the preset split ratio are often much greater[2,3].

Many reasons have been proposed to explain the discrimination and quantitation problems observed in split injections. Broadly these can be grouped into five categories: (a) syringe related problems, such as selective evaporation from the syringe needle[4–7] and non-reproducibility in injection technique[8]; (b) split ratio variations caused by temporal changes in pressure[9–11] or viscosity of the insert mixture[4]; (c) incomplete droplet vaporization[12–14]; (d) non-homogeneity of the resulting sample-carrier mixture[14–16]; and (e) thermal or chemical adsorption[5,6,17]. Experimental

* Present address: Continuum Dynamics, P.O. Box 3073, Princeton, NJ 08543, U.S.A.

0021-9673/88/$03.50 

support for these mechanisms most often is based on the observed variations in peak areas as chromatographic conditions are changed within the experimental design matrix.

A different approach was used in the present work to improve our understanding of the operation of a split injection port: pressure and temperature measurements were made during the injection and a thermodynamic model of the injection process was developed to predict the pressure, flow and temperature variations that occur during an injection.

## EXPERIMENTAL

### *Apparatus and procedure*

A 12.5 m × 0.2 mm I.D. OV-101 column was installed in a Hewlett-Packard Model 5890 A gas chromatograph, and the Hewlett-Packard Model 7673A automated injector was used to make the injections. A Setra Model 205 pressure transducer was connected to the septum purge line six inches from the injection port. The selected transducer had a response time of less than 1 ms. Its volume was filled with an incompressible silicone oil to prevent distortion of the measured pressure pulse[18]. The pressure response was recorded using a digital oscilloscope which was triggered by the pressure increase in the injection port.

Temperature also was measured at several experimental conditions by replacing the capillary column with a thermocouple. The thermocouple response was measured with a Hewlett-Packard 3561 dynamic signal analyzer. Because of the thermal inertia of the approximately 0.3-mm diameter junction the thermocouple response was too slow to measure the temperature changes accurately[19] so the temperature data was used only qualitatively.

A full factorial experiment was designed to investigate the effects on pressure of five variables: injection sample size, injection port temperature, split ratio (or split flow-rate), insert geometry and solvent. A random number table was used to randomize the experimental order to minimize bias and guarantee inferential validity even with unknown sources of variability. Once the experimental conditions were set and the system had equilibrated an injection was made and the pressure and

TABLE I

RANGE OF VARIABLES USED IN EXPERIMENTS

Helium was the carrier gas in all experiments.

| *Variable* | *Range* |
|---|---|
| Sample size (μl) | 1, 3, 4 |
| Initial pressure (kPa) | 68.7 |
| Split flow-rate (ml/min) | 15, 100, 500 |
| Column flow-rate (ml/min) | 1 |
| Injection port temperature (°C) | 100, 200, 400 |
| Insert type (78.5 mm length) | 2 mm I.D. |
| | 4 mm I.D. |
| | 4 mm I.D. Jenning's cup |
| Solvent | Hexane, isooctane |

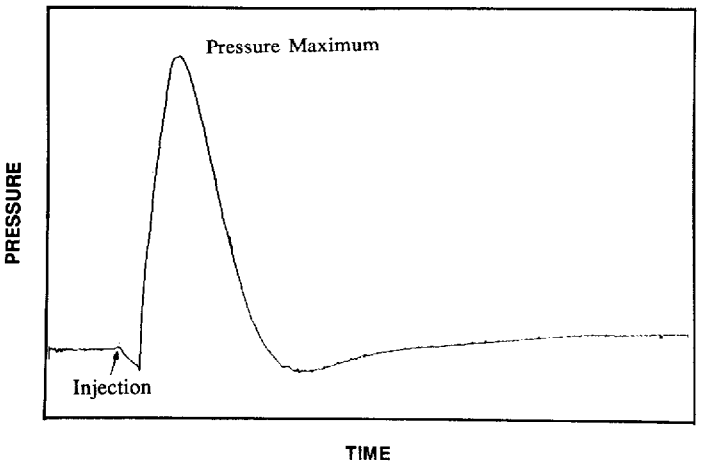


Fig. 1. Characteristic pressure response inside the injection port.

temperature responses were measured and recorded. All of the experimental conditions were replicated. Table I shows the range of experimental conditions that were investigated.

*Experimental results*

A typical pressure response is shown in Fig. 1. The initial pressure decrease was of the order of 0.7 kPa and was followed by a positive pressure change whose magnitude depended on the experimental conditions. The pressure returned to equilibrium after approximately 1 s from the beginning of injection. The specific effects of each variable on the pressure response are summarized as follows: (a) larger sample injections (Fig. 2), and (b) higher injection port temperatures result in larger pressure pulses (Fig. 3), (c) the lower boiling point solvent also yielded larger pressure pulses

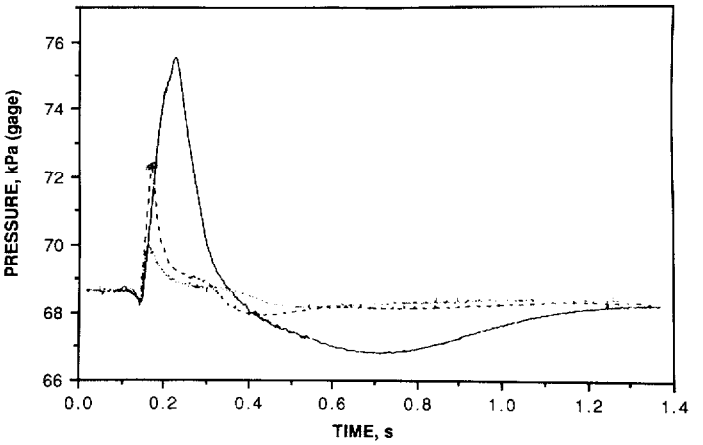


Fig. 2. Effect of sample size on pressure response. Solvent, hexane; wall temperature, 200°C; insert, 4 mm diameter; split flow-rate, 100 ml/min. · · · · ·, 1 μl injection; – – –, 3 μl injection; ——, 5 μl injection.

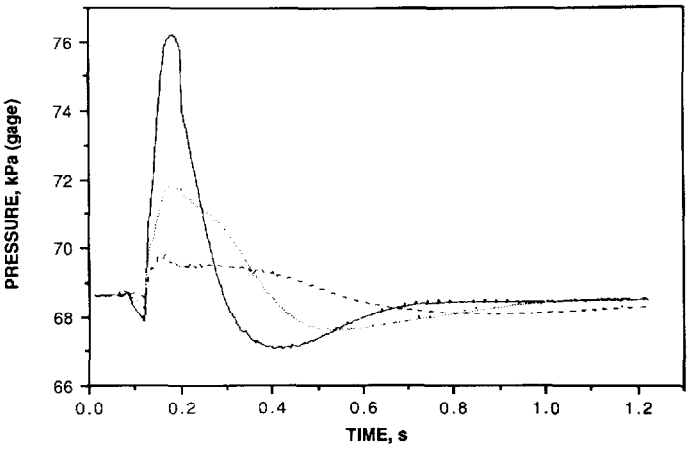


Fig. 3. Effect of wall temperature on pressure response. Solvent, hexane; insert, Jenning's 4 mm; sample size, 3 $\mu$l; split flow-rate, 100 ml/min. – – –, 100°C; · · · · ·, 200°C; ——, 400°C.

(Fig. 4), (d) the split flow-rate did not affect the magnitude of the pressure pulse, but it did have a dramatic effect on the rate at which the pressure returned to equilibrium (Fig. 5). At very low flow-rates the system appeared to be overdamped, while at high flow-rates the pressure undershoots the initial pressure significantly, (e) packed and unpacked 4-mm I.D. liners showed no significant differences in pressure response, except when both the flow-rate and the injection size were at their maximum value (Fig. 6). The similarity of the responses indicates that the packing, for these conditions, had very little impact on the vaporization rate. The pressure amplitudes were much larger in the smaller (2-mm) diameter liner because of the reduced system volume.

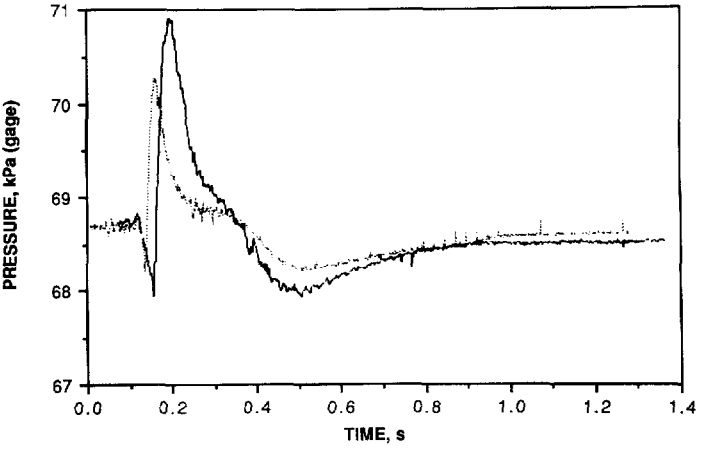


Fig. 4. Effect of solvent on pressure response. Insert, 4 mm diameter; wall temperature, 200°C; sample size, 1 $\mu$l; split flow-rate, 100 $\mu$l/min. ——, Hexane; · · · · ·, isooctane.

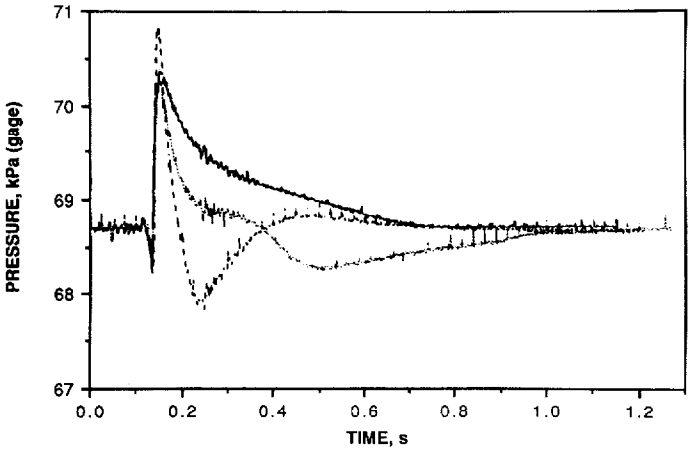


Fig. 5. Effect of split flow-rate on pressure response. Solvent, hexane; insert, 4 mm diameter; sample size, 1 $\mu$l; wall temperature, 200°C. ——, 15 ml/min; · · · · ·, 100 ml/min; – – –, 500 ml/min.

## THERMODYNAMIC MODEL

Uniform property but time dependent control volume analysis of the injection port was used to model the pressure and temperature responses. For this purpose the injection port, which is represented schematically in Fig. 7, was divided into three control volumes: (a) the insert control volume for which the liquid sample represents a source of mass and a sink of energy due to the vaporization process, (b) the mass flow controller (MFC) control volumes, and (c) the back pressure regulator (BPR) control volume. The first of the three control volumes represents the temperature-controlled insert, while the last two represent the tubing and miscellaneous other volumes

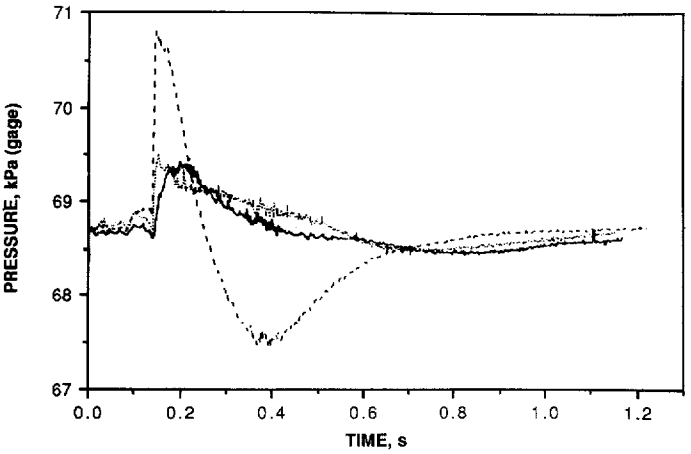


Fig. 6. Effect of different inserts on pressure response. Solvent, hexane; sample size, 1 $\mu$l; wall temperature, 100°C; split flow-rate, 100 $\mu$l/min. – – –, 2 mm insert; ——, 4 mm insert; ···· Jenning's insert, 4 mm.

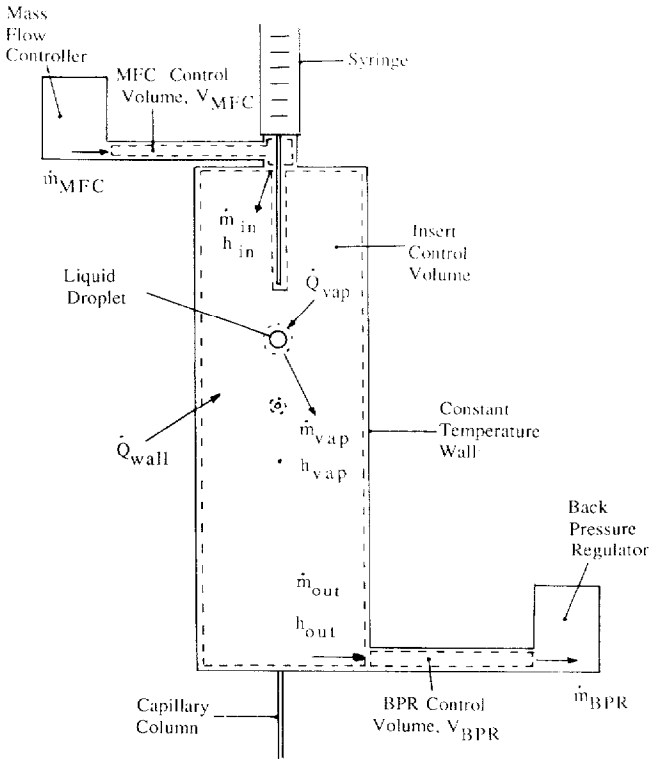


Fig. 7. Schematic representation of split injection port and associated control volumes.

associated with the MFC and BPR, respectively. A mass balance for the insert control volume can be written as follows:

$$\dot{m}_{in} + \dot{m}_{vap} - \dot{m}_{out} = \dot{m}_{cv} \tag{1}$$

where $\dot{m}_{in}$ and $\dot{m}_{out}$ are the mass flow-rates in and out of the insert control volume, respectively, $\dot{m}_{vap}$ is the sample vaporization rate, and $\dot{m}_{cv}$ is the rate of change of mass in the insert control volume. Assuming the carrier gas and sample vapor are homogeneously mixed ideal gases inside the insert volume, $V$, eqn. 1 can be written as

$$\dot{m}_{cv} = \frac{V}{RT}\frac{dP}{dt} - \frac{PV}{R^2T}\frac{dR}{dt} - \frac{PV}{RT^2}\frac{dT}{dt} \tag{2}$$

where $P$ and $T$ are the uniform insert pressure and temperature, respectively, and $R$ is the instantaneous mixture gas constant. Similar mass balances for the BPR and MFC can be used for evaluating $\dot{m}_{in}$ and $\dot{m}_{out}$, respectively. Substituting the resulting expressions in eqn. 2, and solving for $dP/dt$ yields

$$\frac{dP}{dt} = \frac{\frac{RT}{V}(\dot{m}_{MFC} + \dot{m}_{vap} - \dot{m}_{BPR}) + \frac{P}{T}\frac{dT}{dt} + \frac{P}{R}\frac{dR}{dt}}{\left(1 + \frac{TV_{MFC}}{T_{MFC}t} + \frac{TV_{BPR}}{T_{BPR}V}\right)} \tag{3}$$

where $\dot{m}_{MFC}$, and $V_{MFC}$ are the inlet mass flow-rate and volume of the MFC, and $\dot{m}_{BPR}$, and $V_{BPR}$ are the outlet mass flow-rate and volume of the BPR, respectively. In deriving eqn. 3 it was assumed that the temperatures of the gas in the MFC, $T_{MFC}$, and BPR, $T_{BPR}$, are approximately equal to the mean temperature between the insert and the ambient temperatures. This assumption was used for simplicity and does not affect the character of the predicted response by the model, but only has a small effect in the scaling of the pressure and temperature maxima and minima.

Regarding the mass flow-rates in eqn. 3 it is assumed that the mass flow controller behaves ideally, which implies that $\dot{m}_{MFC}$ remains constant regardless of downstream pressure variations. The back pressure regulator is assumed to act as a second order regulator with $\dot{m}_{BPR}$ given by the pressure and time-dependent expression shown in Appendix 1. The sample vaporization rate, $\dot{m}_{vap}$ is modeled assuming that the syringe injector produces a stream of spherical droplets which all have an initial diameter equal to the syringe inside diameter. This assumption is made in the absence of initial droplet size data for samples ejected by the syringe system used and appears to be an adequate idealization in view of the reasonable pressure and temperature responses that were computed. The droplets according to the $D^2$ law with the vaporization constant computed from quasi-steady theory[20] using the relations shown in Appendix 2. The time derivative of the mixture gas constant $R$ requires knowledge of the carrier gas and sample vapor masses inside the insert volume. These are given by the following relationships:

$$\dot{m}_s = \dot{m}_{vap} - [m_s/(m_s + m_c)]\dot{m}_{out}$$

$$\dot{m}_c = \dot{m}_{in} - [m_s/(m_s + m_c)]\dot{m}_{out} \tag{4}$$

where $m_s$ and $m_c$ are the sample and carrier gas masses in the insert volume, and $\dot{m}_s$ and $\dot{m}_c$ are their time derivatives.

Evaluation of $dT/dt$ in eqn. 3 requires an energy balance on the insert control volume. Using Fig. 7 this can be written as follows:

$$\dot{m}_{in}h_{in} + \dot{m}_{vap}h_{vap} - \dot{Q}_{vap} - \dot{m}_{out}h_{out} + \dot{Q}_{wall} = \dot{E}_{cv} \tag{5}$$

where $h_{in}$ and $h_{out}$ are the enthalpies of the entering carrier gas and exiting mixture, respectively, $h_{vap}$ is the enthalpy of the sample vapor at the temperature of the control volume, $\dot{Q}_{vap}$ is the energy rate required to vaporize the sample, $\dot{Q}_{wall}$ is the rate of energy addition from the liner wall and $\dot{E}_{cv}$ is the rate of energy change in the insert control volume. Heat transfer to the syringe is neglected. For an ideal gas $\dot{E}_{cv} = d(m_{cv}c_vT)/dt$ where $c_v$ is the instantaneous mixture specific heat at constant volume. Substituting this expression into eqn. 5 and solving for $dT/dt$ yields

$$\frac{dT}{dt} = \frac{1}{m_{cv}c_v}(\dot{m}_{in}h_{in} - \dot{m}_{out}h_{out} + \dot{m}_{vap}h_{vap} - \dot{Q}_{vap} + \dot{Q}_{wall}) -$$

$$+ \frac{T}{m_{cv}}\frac{dm_{cv}}{dt} - \frac{T}{c_v}\frac{dc_v}{dt} \quad (6)$$

The heat transfer coefficient, $h$, from the insert wall can be estimated using the Nusselt number for fully developed flow in an isothermal tube, $hD/k = 3.66$, where $k$ is the temperature-dependent thermal conductivity of the gas mixture. However, the value of the resulting heat transfer coefficient was too small to provide good correlation with the peak pressure experimental values. A value of 5 h was empirically found to yield better agreement with the experimental results and was used for all calculations. This can be justified because some sample droplets may impinge on the wall producing better mixing and heat transfer than that predicted by the fully developed laminar flow relation. The pure component enthalpies in eqn. 6 are evaluated using the ideal gas assumption, and $h_{out}$ is the resulting mixture enthalpy. $c_v$ and its derivative are obtained for the mixture in a similar fashion.

## RESULTS AND DISCUSSION

The two coupled differential equations, eqns. 3 and 6, together with the previously discussed necessary auxiliary relations were integrated numerically for the experimental conditions tested, using the constants in Table II. Physical properties were obtained from ref. 21. Typical results for the pressure and temperature responses are shown in Figs. 8 and 9, respectively, where they are also compared with experimental data. The evolution of the pressure response to an injection is described below. It appears that the initial pressure decrease was caused by the temperature reduction which occurred as a result of energy transfer from the gas to the sample. As the temperature difference between the liner wall and the gas increased more heat was convected from the wall. This energy, combined with the increased mass from the sample vaporization process caused the pressure in the insert to increase. As the pressure approached its maximum value the response of the back pressure regulator became dominant reducing the pressure in the injection port by increasing $\dot{m}_{out}$ and accounting for the return to equilibrium conditions. The return to equilibrium pressure is the portion of the response where the difference between the experimental data and the model was greatest, indicating that a better model for the back pressure regulator is needed. Comparisons for different operating conditions showed good agreement between computed and measured pressure responses for the initial pressure response with similar difficulties in estimating the response of the back pressure regulator. Regarding the temperature response in Fig. 9, although there is qualitative agreement between computed and measured results, the measured temperatures lag the computed values. The previously mentioned thermal inertia of the thermocouple junction is a probable reason for the lag.

The split ratio is defined as the ratio of split flow (through the back pressure regulator) to column flow. The column flow, $Q_c$, can be computed assuming

TABLE II

PARAMETER VALUES USED IN CALCULATIONS

| *Parameter* | *Value* |
|---|---|
| Back pressure regulator control volume ($V_{BPR}$) ($cm^3$) | 0.7 |
| Mass flow controller control volume ($V_{MFC}$) ($cm^3$) | 0.7 |
| Initial sample droplet size ($D_0$) ($\mu$m) | 150 |
| Length of column ($L$) (m) | 12.5 |
| Column radius ($r_c$) (mm) | 0.25 |

incompressible, laminar, constant viscosity flow with negligible mass transfer to the column liquid phase

$$\dot{Q}_c = \frac{\pi r_c^4}{8\mu}\frac{dp}{dx} \tag{7}$$

where $\mu$ is the viscosity, $r_c$ is the column radius and $dp/dx$ is the constant pressure gradient. Therefore, the split ratio (SR), written in terms of the mass flows is

$$SR = \frac{8\dot{m}_{out}\mu L}{\pi\rho r_c^4(P - P_{atm})} \tag{8}$$

where $L$ is the column length, $\rho$ is the gas density and $(P - P_{atm})$ is the instantaneous difference in pressure between the liner and the surroundings. Fig. 10 shows that the predicted split ratio using eqn. 8 differs significantly from the preset steady-state value.

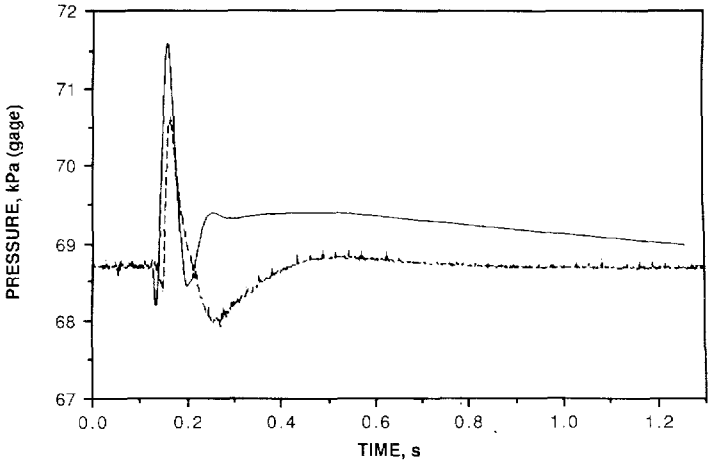


Fig. 8. Predicted (——) *vs.* experimental (– – –) pressure response. Solvent, hexane; sample size, 1 $\mu$l; insert, 4 mm diameter; wall temperature, 200°C; split flow-rate, 500 ml/min.

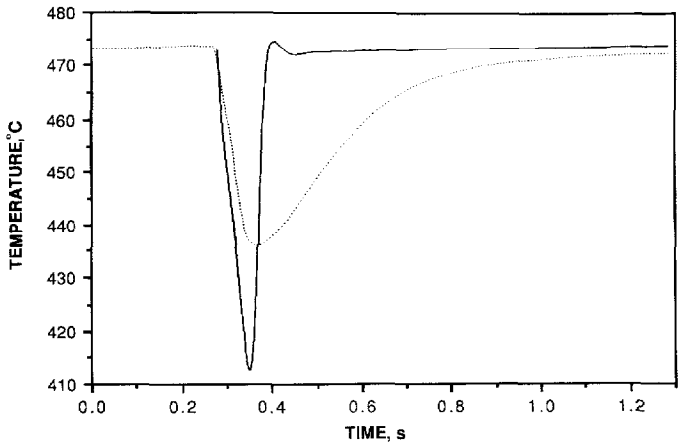


Fig. 9. Predicted (——) *vs.* experimental (· · · · ·) temperature response. Solvent, hexane; sample size, 5 μl; insert, 4 mm diameter; wall temperature, 200°C; split flow-rate, 500 ml/min.

In general, to determine the discrimination or quantitative errors associated with the variable split ratio the mass of each solute at the split point must be known as a function of time. Then integration of the split ratio weighted by the mass distribution at the split point yields the average split ratio for the solute of interest:

$$\overline{\mathrm{SR}} = \frac{1}{\Delta T} \int_0^{\Delta T} m(t)\ \mathrm{SR}(t)\ \mathrm{d}t \tag{9}$$

where $\Delta T$ is the time the solute is split, $m(t)$ is the time varying fraction of the total mass of the solute at the split point and $\mathrm{SR}(t)$ is the time varying split ratio. Accurate

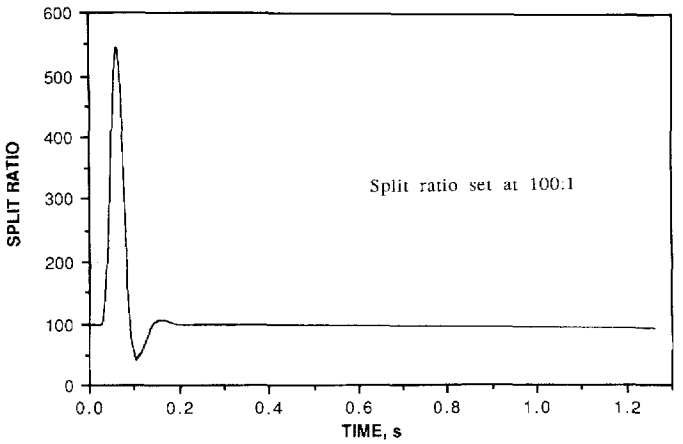


Fig. 10. Predicted split ratio response. Solvent, hexane; sample size, 1 μl; insert, 4 mm diameter; wall temperature, 200°C; split flow-rate, 100 ml/min.

estimation of $m(t)$ requires knowledge of the local vapor concentration within the insert, which is not included in the present model. However, a single component example can be used to illustrate how this model can be used to quantify split ratio errors, using the conditions for the injection depicted in Fig. 10. The hexane vapor fraction at the split point will be assumed to be normally distributed and split completely within 1 s, which is approximately the time required to purge the insert volume twice. Performing the integration indicated in eqn. 9 yields an average split ratio of 106:1 instead of the anticipated 100:1. This 6% error will vary depending on the actual $m(t)$ and $SR(t)$ for a particular injection.

An additional use of the present model is to evaluate alternate injection port designs. For example, alternate flow systems can be studied by substituting appropriate response functions for $\dot{m}_{MFC}$ and $\dot{m}_{BPR}$ in the equations. Different insert geometries can be investigated by varying the volume and heat transfer coefficient of the insert.

## CONCLUSIONS

The pressure and temperature changes that occur during injection in a split injection port were measured. The experimental data was then compared to the results of a thermodynamic model which qualitatively predicted all of the important features of the pressure and temperature responses seen in the experimental data. The model was then extended to predict the variations that occur in the split ratio.

Coupling the model with a simulation of the time varying solute distribution in the insert would allow the average split ratio of each solute to be predicted. Future work to extend and improve the model should include a better response model for the back pressure regulator, improved sample vaporization modeling to handle realistic sample mixtures and a better simulation of the column flow.

## ACKNOWLEDGEMENT

We gratefully acknowledge the scholarship support and the loan of laboratory equipment provided by the Avondale Division of Hewlett-Packard Company in Avondale, PA, U.S.A.

## APPENDIX I

*Response of the back pressure regulator*

The BPR controls the upstream pressure by allowing a variable flow-rate through a nozzle flapper assembly. Masters[22] has shown that the flow response of a BPR is highly non-linear and depends on parameters which were unknown for the BPR employed in the present work. Therefore, the BPR was modeled as a second order regulator with a natural frequency ($w_n$ = 80 radians/s) and a damping coefficient ($b$ = 0.55) determined from experimental measurements. Further, it was assumed that the forcing function disturbing the BPR was the increase in pressure from the evaporation process and that when the pressure began to decrease the forcing function stopped and the BPR responded freely. The forcing function was approximated by a series of impulses each with an amplitude equal to a constant multiplied by the

pressure difference between the actual and set pressure. The volumetric flow response, Flow($t$), of this second order regulator to an impulse of amplitude $A$ was therefore expressed as:

$$\text{Flow}(t) = Aw_n/(1 - b^2) \exp(-bw_n t) \sin[w_n(1 - b^2)t] \tag{A1}$$

where $t$ is the time. The total mass flow-rate out of the BPR is the initial mass flow-rate plus the gas density multiplied by the sum of the dynamic responses. Therefore

$$\dot{m}_{BPR} = \dot{m}_{in} + \rho\Sigma[\text{Flow}(t)] \tag{A2}$$

## APPENDIX II

*Droplet vaporization rate*

The mass vaporization rate of a droplet can be related to the diameter change by

$$\dot{m}_{drop} = -\frac{\pi}{4}\rho_l D \frac{dD^2}{dt} \tag{A3}$$

where $\rho_l$ and $D$ are the liquid density and diameter of the droplet, respectively. Using the $D^2$ evaporation law [20]

$$D^2 = D_0^2 - e_{vap}t \tag{A4}$$

where $D_0$ is the initial sample droplet size, results in

$$\frac{dD^2}{dt} = -e_{vap} \tag{A5}$$

where $e_{vap}$ is the vaporization constant. For small droplets in a hot ambient gas ref. 20 gives the following relation for $e_{vap}$

$$e_{vap} = \frac{8\rho_g\alpha_g}{\rho}\ln(B + 1) \tag{A6}$$

where $\rho_g$ and $\alpha_g$ are the density and thermal diffusivity of the gas and $B$ is defined as

$$B = c_p(T - T_S)/L = (-Y_\infty + Y_{FS})/(1 - Y_{FS}) \tag{A7}$$

where $c_p$ is the gas specific heat at constant pressure, $T_S$ is the saturation temperature of the sample vapor, $L$ is the latent heat of vaporization of the droplet, $Y_{FS}$ is the mass fraction of sample vapor at the droplet surface and $Y_\infty$ is the sample vapor mass fraction far away from the droplet. In the present case $Y_\infty$ was set to zero and the Clausius–Clapeyron equation was used to relate $Y_{FS}$ and $T_S$

$$Y_{FS} = \frac{M_S}{M_M} \exp\left[\frac{LM_S}{R}\left(\frac{1}{T_B} - \frac{1}{T_S}\right)\right] \tag{A8}$$

where $M_S$ is the molecular weight of the sample, $M_M$ is the molecular weight of the mixture, $T_B$ is the boiling point of the sample, and $L$ is its latent heat of vaporization. By substituting eqn. A8 into eqn. A7, $T_S$ can be found using any iterative method. Substituting this value of $T_S$ into eqn. A7 yields the value of $B$ from which $e_{vap}$ and $\dot{m}_{drop}$ can be calculated. The total vaporization rate, $\dot{m}_{vap}$, is given by summing up the vaporization rate of all droplets present.

## REFERENCES


1 K. Grob and S. Rennhard, *J. High Resolut. Chromatogr. Chromatogr. Commun.*, 3 (1980) 627.
2 G. Schomburg, H. Husmann and R. Rittmann, *J. Chromatogr.*, 204 (1981) 85.
3 K. Grob and K. Grob, Jr., *J. Chromatogr.*, 151 (1978) 311.
4 K. Grob, Jr., in R. E. Kaiser (Editor), *Capillary Chromatography, Fourth International Symposium, Hindelang, 1981*, Institute of Chromatography, Bad Dürkheim, 1981, p. 185.
5 G. Schomburg, in R. E. Kaiser (Editor), *Capillary Chromatography, Fourth International Symposium, Hindelang, 1981*, Institute of Chromatography, Bad Dürkheim, 1981, p. 371.
6 K. Grob, Jr. and H. P. Neukan, *J. High Resolut. Chromatogr. Chromatogr. Commun.*, 2 (1978) 15.
7 F. Poy, S. Visani and F. Terrosi, *J. Chromatogr.*, 217 (1981) 81.
8 D. W. Grant and A. Clarke, *J. Chromatogr.*, 97 (1974) 115.
9 F. Munari and S. Trestianu, in R. E. Kaiser (Editor), *Capillary Chromatography, Fourth International Symposium, Hindelang, 1981*, Institute of Chromatography, Bad Dürkheim, 1981, p. 849.
10 H. Brudereck, W. Schneider and I. Halasz, *J. Gas Chromatogr.*, 5 (1967) 217.
11 K. Grob, Jr. and H. P. Neukom, *J. High Resolut. Chromatogr. Chromatogr. Commun.*, 2 (1979) 563.
12 G. Schomburg, H. Behlau, R. Dielmann, F. Weeke and H. Husmann, *J. Chromatogr.*, 142 (1972) 87.
13 A. L. German and E. C. Horning, *Anal. Lett.*, 5 (1972) 619.
14 C. Watanabe, H. Tomita and N. Sato, in R. E. Kaiser (Editor), *Capillary Chromatography, Fourth International Symposium, Hindelang, 1981*, Institute of Chromatography, Bad Dürkheim, 1981, p. 499.
15 M. J. Hartigan and L. S. Ettre, *J. Chromatogr.*, 119 (1976) 187.
16 L. S. Ettre, *Introduction to Open Tubular Columns*, Perkin-Elmer, Norwalk, CT, 1979.
17 J. Eyem, *J. Chromatogr.*, 217 (1981) 99.
18 G. White, *Instrument Notes*, Statham Labs., Los Angeles, CA, 1949, p. 7.
19 A. Kaufman, *Masters Thesis*, Rutgers University, Piscataway, NJ, 1987.
20 M. Kanury, *Introduction to Combustion Phenomenon*, Gordon and Breach, New York, 1975.
21 R. Reid and T. Sherwood, *Properties of Gases and Vapors*, McGraw-Hill, New York, 1966.
22 C. A. Masters, *Dynamic Characteristics of a Restrictor Compensated Nozzle/Flapper Pressure Transducer*, Department of Chemical Engineering, Northwestern University, Evanston, IL, 1974.